Spatiotemporal Oxygen Sensing Using Dual Emissive Boron Dye–Polylactide Nanofibers
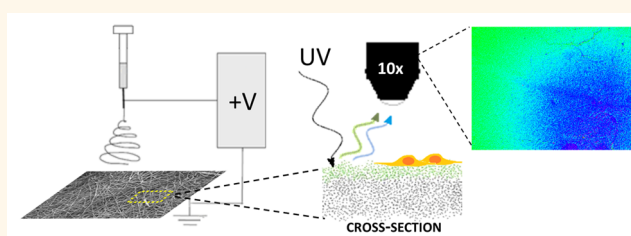
Daniel T. Bowers,[†] Michael L. Tanes,[‡] Anusuya Das,[†,§] Yong Lin,[†] Nicole A. Keane,[†] Rebekah A. Neal,[†] Molly E. Ogle,[‡] Kenneth L. Brayman,[†,⊥] Cassandra L. Fraser,[†,‖] and Edward A. Botchwey*,[†,‡]

[†]Department of Biomedical Engineering, University of Virginia, Charlottesville, Virginia 22908, United States, [‡]Wallace H. Coulter Department of Biomedical Engineering, Georgia Institute of Technology and Emory University, Atlanta, Georgia 30332, United States, [§]Orthopaedic Surgery, University of Virginia, Charlottesville, Virginia 22908, United States, [⊥]Department of Surgery, University of Virginia, Charlottesville, Virginia 22908, United States, and [‖]Department of Chemistry, University of Virginia, Charlottesville, Virginia 22908, United States

ABSTRACT Oxygenation in tissue scaffolds continues to be a limiting factor in regenerative medicine despite efforts to induce neovascularization or to use oxygen-generating materials. Unfortunately, many established methods to measure oxygen concentration, such as using electrodes, require mechanical disturbance of the tissue structure. To address the need for scaffold-based oxygen concentration monitoring, a single-component, self-referenced oxygen sensor was made into nanofibers. Electrospinning process parameters were tuned to produce a biomaterial scaffold with specific morphological features. The ratio of an oxygen sensitive phosphorescence signal to an oxygen insensitive fluorescence signal was calculated at each image pixel to determine an oxygenation value. A single component boron dye—polymer conjugate was chosen for additional investigation due to improved resistance to degradation in aqueous media compared to a boron dye polymer blend. Standardization curves show that in fully supplemented media, the fibers are responsive to dissolved oxygen concentrations less than 15 ppm. Spatial (millimeters) and temporal (minutes) ratiometric gradients were observed *in vitro* radiating outward from the center of a dense adherent cell grouping on scaffolds. Sensor activation in ischemia and cell transplant models *in vivo* show oxygenation decreases on the scale of minutes. The nanofiber construct offers a robust approach to biomaterial scaffold oxygen sensing.

KEYWORDS: nanofibers · electrospinning · ratiometric · oxygen · hypoxia · scaffold · cell transplant

Spatial oxygen gradients drive many cellular functions including cell migration,[1] signaling,[2−4] and differentiation.[5] Sustained low oxygen tensions in tissue can impair the regenerative capacity and survival of tissue engineered grafts.[6,7] Therefore, the measurement of local oxygen concentration within a three-dimensional cell adherent scaffold is valuable in studying and tuning the dynamics of engineered graft success and integration. In this study, dual emissive boron dyes were used as ratiometric oxygen sensors to enable understanding of the dynamic aspects of oxygen gradient responses in a noninvasive manner. While other oxygen sensing dyes have been utilized for real-time cell imaging, many require separate fluorophore standards that can be subject to differential degradation and

photobleaching,[8,9] which may compromise their longevity and dynamic precision *in vivo*. The boron dyes used in the current study emit an oxygen-sensitive phosphorescence signal and an oxygen-independent fluorescence signal.[10−12] The ratio of the phosphorescence to the fluorescence (*P/F* ratio) produces an internally standardized ratiometric detection of molecular oxygen.

Several oxygen sensors have been blended with polyurethane,[13] polystyrene,[14−17] and polycaprolocone (PCL),[18] to make micro- and nanoscale biomaterials. The current study compares polymer blended and polymer-conjugated forms of the oxygen sensitive single component boron-dye in electrospun nanofibers. The small diameter and large surface to volume ratio of nanofibers provides a small distance for oxygen

diffusion within the polymer matrix to reach an embedded molecular sensor. Furthermore, the nanofiber structure of the biomaterial provides the advantage of extracellular matrix (ECM) mimetic morphology[19] over previous boron dye formulations in nanoparticle form.[11,12] Electrospinning is an ideal method for synthetic tissue engineering scaffold production because it allows tuning of the process parameters to create scaffolds of controlled morphology that are beneficial for the culture and control of many cell types such as Schwann cells,[20,21] oligodendrocytes,[22] neural progenitors,[23,24] neurites,[25] cardiomyocytes,[26] osteoblasts,[27] human skin fibroblasts,[28] smooth muscle cells or endothelial cells,[29] hepatocytes,[30] mesenchymal stem cells,[31−34] embryonic stem cells[35−37] and induced pluripotent stem cells.[37,38]

This study explores the nanofabrication and material properties of blended[39] and conjugated[10] formulations of the boron dye electrospun into nanofibers for their application in biological research. Tissue engineering scaffolds must function in aqueous environments for periods of time from hours to weeks depending on the application. Spectrophotometric characterization of the dye and poly(lactic-*co*-glycolic acid) (PLAGA) blend nanofiber scaffolds in this and other[39] studies revealed low phosphorescence signal before and after exposure to aqueous media. This study then explores a poly(lactic acid) (*i.e.*, polylactide) conjugated form of the boron dye as a method to improve performance of the tissue engineering scaffold. The polymer conjugated form of the dye was validated by calibration against various levels of hypoxia. Then the dye-polymer conjugate nanofiber scaffold was utilized to detect oxygen variation *in vitro* and using hypoxia models *in vivo*. This material presents a useful tool in the real-time detection of localized oxygen gradients that could provide valuable information in the context of tissue engineering applications.

RESULTS AND DISCUSSION

PLAGA and Boron Dye Blend Nanofibers. While biodegradable electrospun polymer nanofibers have been characterized in the literature,[40] the performance of the boron dye when blended with PLAGA or conjugated to a polymer in a nanofiber scaffold had not been investigated. The oxygen sensitive dye (BF$_2$dbm (I)OH) was first blended with the aqueous degradable 50:50 PLAGA (lactic/glycolic subunits) polymer to make electrospun nanofibers. Oxygen sensing capability was assessed after incubation in phosphate buffered saline (PBS) filled microtubes at 37 °C in a shaking water bath, by comparing phosphorescence and fluorescence signals (peaks at 525 and 450 nm, respectively). The 50:50 PLAGA dye blend nanofiber scaffold exhibited a reduced oxygen sensing ability after a week which could be a result of polymer degradation (Figure 1a).[39]
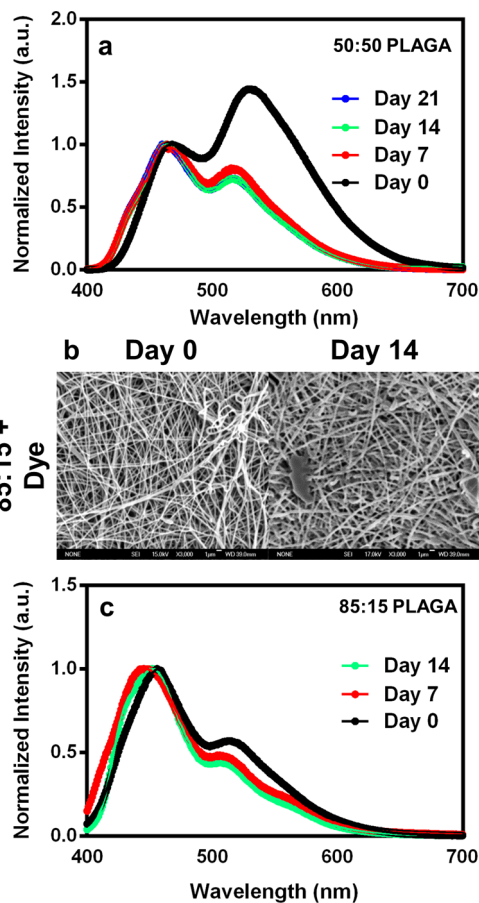

Figure 1. Boron-dye polymer blend sensor spectral response to low oxygen after incubation in aqueous media for polymer blend nanofibers of 50:50 PLAGA at 0, 7, 14, and 21 days ((a) samples were lyophilized after indicated time in aqueous media and read in a nitrogen purged environment). Fiber morphology of the 85:15 PLAGA dye blend nanofibers was maintained over a 14 day degradation study (b). Sensor spectral response to low oxygen environment (85:15 PLAGA dye blend at 0, 7, and 14 days) (c).

To address this issue, we hypothesized that replacing the 50:50 PLAGA with the slower degrading 85:15 PLAGA would protect the oxygen sensing ability of the dye in the electrospun blend nanofiber scaffold over time.[41] Gel-permeation chromatography was conducted after 1, 2, or 3 weeks of incubation in PBS by lyophilizing the sample which could then be dissolved in an organic solvent. In comparison to the 50:50 ratio, the 85:15 ratio indeed degraded more slowly and the addition of BF$_2$dbm(I)OH dye had little effect on polymer chain shortening (Supporting Information Table S1). The microstructure of the 85:15 scaffolds was maintained following incubation in aqueous media for 14 days (Figure 1b and Supporting Information Figure S2). Shifts in the room temperature phosphorescence peak suggest changes in the dye microenvironment. We observed the phosphorescence peak blue-shifted twice as much in the 50:50 copolymer ratio compared to the 85:15 copolymer ratio (Supporting Information Table S2 and Figure S1), suggesting better
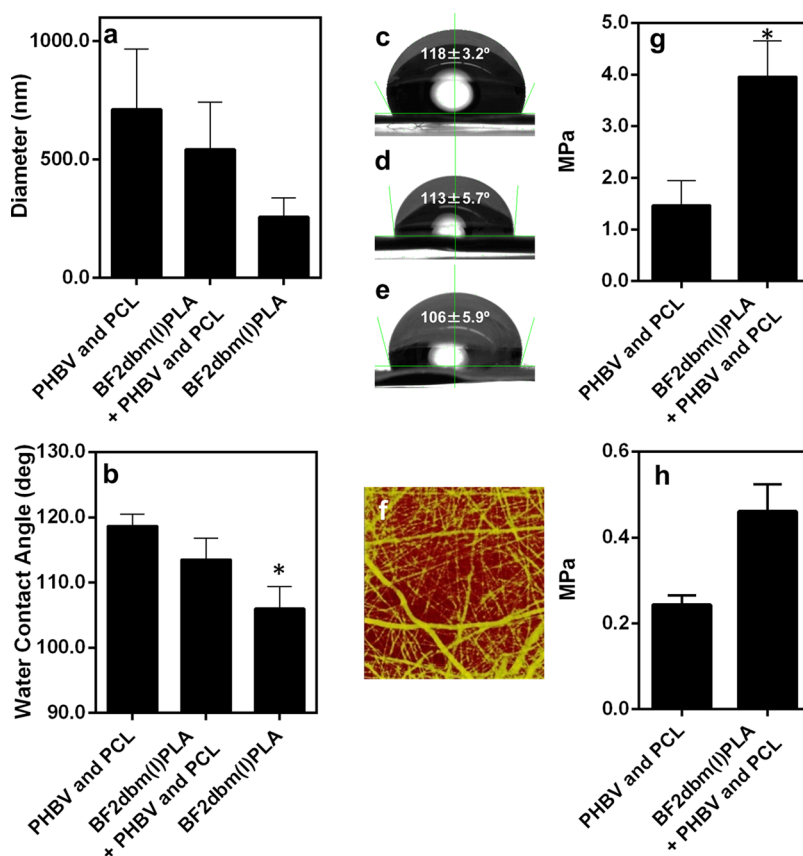
Figure 2. Nanofiber diameter for the three materials ((a) mean $\pm$ standard deviation). The water contact angle measurements of the three materials ((b) $n = 3$ for each group, mean $\pm$ standard error, $*p < 0.05$ compared to PHBV and PCL fibers), images ((c) PHBV and PCL fibers; (d) PHBV and PCL boron dye-polymer conjugate dual layer scaffold; (e) boron dye PLA Fibers, mean $\pm$ standard deviation). Confocal microscopy shows the boron dye-polymer conjugate layer (light green) over the PHBV and PCL layer (deep red) (f). Young's modulus (g) and ultimate tensile strength (h) suggest the boron dye-polymer conjugate layer attaches to the PHBV and PCL layer ($n = 3$ for each group, mean $\pm$ standard error, $*p < 0.05$).

preservation of dye microenvironment with the slower degrading polymer. Despite the slower degradation properties of 85:15 PLAGA, the scaffold phosphorescence peak was weak in comparison to the fluorescence peak after fabrication (Day 0) and after weeks of *in vitro* aqueous exposure (Figure 1c), which reduces the utility of the scaffold for ratiometric imaging in tissue engineering applications. Therefore, the boron dye polymer blend nanofiber scaffolds were not investigated further in this study.

Dual Layer Scaffold Construction for Tissue Engineering. In the blended PLAGA and dye nanofibers, diffusion of the dye in the polymer matrix[42] and enhanced dye degradation by hydrolysis may contribute to the loss of scaffold oxygen sensing function over time in aqueous media. To reduce diffusional loss of oxygen sensor to the surrounding aqueous media and to preserve sensor function, a form of the dye that is chemically conjugated to a poly(lactic acid) (PLA) polymer[10] replaced the physical mixture of dye and polymer for scaffold fabrication. The PLA-conjugated boron dye (BF$_2$dbm(I)PLA) selected for this study, which had been synthesized previously,[10] has a relatively low molecular weight for electrospinning (13 kDa) requiring extra

parameter adjustment to produce fibers of consistent morphology. Optimization of the electrospinning process yielded final parameters of 30% (w/v) dye—polymer conjugate in 10% (v/v) pyridinium formate, 20% (v/v) ethanol, in dichloromethane at a 25 kV applied voltage, 14.5 cm working distance, and 1 mL/h solution flow rate applied to the 13 kDa PLA alone and the boron dye—polymer conjugate (Supporting Information Figure S3).

The dye—polymer conjugate (BF$_2$dbm(I))PLA) nanofiber mat was fragile in handling for experiments. It was therefore necessary to reinforce the mat with a structural support layer. Blended poly(3-hydroxybutyrate-*co*-3-hydroxyvalerate) and polycaprolactone (PHBV and PCL) nanofibers were employed (Supporting Information Figure S3) as the structural layer to create a dual layer tissue engineering scaffold. The dye-polymer conjugate nanofibers were electrospun onto the dry PHBV and PCL nanofibers attached to the grounded collector plate (Supporting Information Figure S3), allowing for the simultaneous removal and handling of the supporting and sensing nanofiber layers.

The dual layer scaffold had an intermediate nanofiber diameter between the mean diameter of the
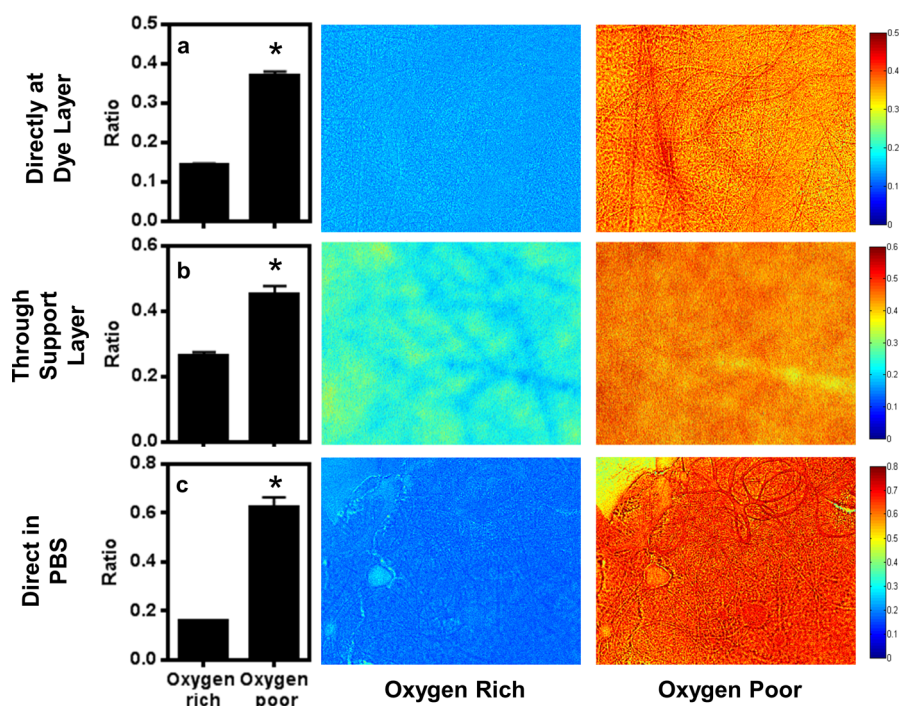
Figure 3. Ratiometric imaging of the dual layer scaffold with the support layer opposite the dye-polymer conjugate layer from the microscope objective (a), and with the support layer between the objective and the dye layer (b) was found to be similar. Submersion in PBS with the dye layer closest to the microscope objective (c) demonstrates that the dye-polymer conjugate nanofibers are still functional in a buffered media ($n = 5$, standard error of the mean shown, $*p < 0.05$, two-tailed independent means t test).

support layer or the dye-polymer conjugate layer alone (Figure 2a). The water contact angle of the dye layer was significantly lower than the support layer and the dual layer scaffold had an intermediate value between either individual layer (Figure 2b—e). Fluorescence confocal microscopy of the surface of the dual layer scaffold demonstrate both layers have surface exposure as evidenced by only partial surface coverage of green (dye-polymer conjugate) over the red (PHBV and PCL) fluorescence (Figure 2f). Therefore, cells growing on the scaffold are expected to experience the material properties of both layers.

The Young's Modulus of the nanofiber substrate can affect the phenotype of cells cultured on the material.[43−45] To test the tensile properties of the dye-polymer conjugate nanofiber mat, we compared the dual layer scaffold to the PHBV and PCL support layer alone. The Young's Modulus of the dual layer scaffold was greater than the support layer alone (Figure 2g). Cells that are grown on the dual layer scaffold are therefore expected to experience two different values of stiffness. Tissue engineering applications exert various forces on scaffolds including tensile loads. The addition of the dye-polymer conjugate layer caused the ultimate tensile strength to be slightly greater than the PHBV and PCL scaffold alone (Figure 2h). The inability to handle the dye fibers alone then may result from the thin nature of the layer and perhaps bending forces applied during peeling

rather than a lack of strength of the material. Being attached to a thicker, lower Young's Modulus layer endows the ability to handle the dye scaffold and gives two cell substrates to the scaffold.

To test whether the dual layer dye-polymer conjugate nanofiber scaffold can register changes in oxygen levels in different environments, ratiometric imaging was conducted in dry atmosphere (Figure 3a,b) or PBS (Figure 3c). The scaffold was exposed to an oxygen rich or oxygen poor environment with the dye side imaged directly (Figure 3a,c) or through the support layer (Figure 3b). The increase from an oxygen rich P/F ratio to an oxygen poor P/F ratio was still detected when imaging through the dual layer scaffold, confirming that the scaffold can be used in either orientation if the changes in ratio are all that is desired. Further, similar ratios were measured when the scaffold was submersed in PBS (Figure 3c), confirming signal generation in a hydrated environment. Fiber morphology is obscured when imaging through the support layer; therefore, in the validation experiments the dye side is imaged directly to ensure that the best possible spatial resolution was obtained.

Performance Stability of Boron Dye Conjugate Nanofibers. To understand the effects of long-term exposure to aqueous media which is critical to cell culture and *in vivo* applications, the spectral response of the dye-polymer conjugate dual layer scaffold was measured after 0, 7, 14, and 21 days of incubation in PBS at
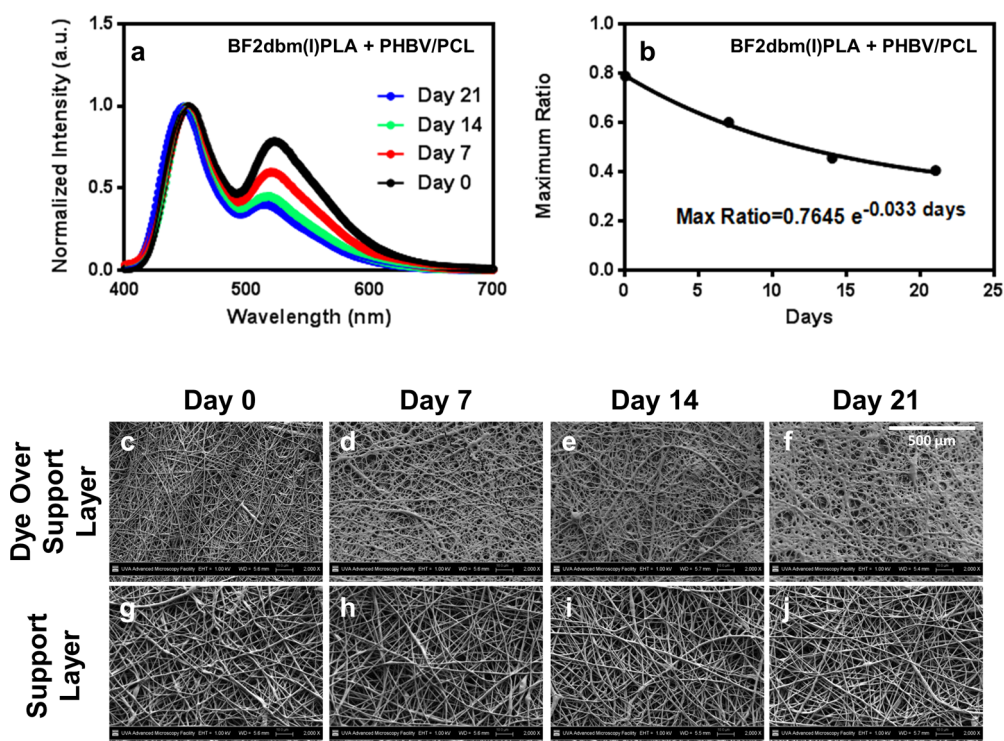
Figure 4. Boron-dye sensor spectral response to low oxygen in dye—polymer conjugate nanofibers after incubation in aqueous media (a) ($n = 6$ per time point) for 0, 7, 14, and 21 days (dual layer scaffold samples were lyophilized after indicated time in aqueous media and read in a nitrogen purged environment). Regression calculated exponential decay of polymer conjugate scaffold sensor maximum ratio after aqueous incubation for 7, 14, and 21 days (b). Under scanning electron microscopy, the dye-polymer conjugate sensor layer swelled with time in aqueous media (c—f) while the support fibers maintained their structure (g—j). Scale bar 500 μm.

physiological temperature. The intensity of the phosphorescence peak of the dye-polymer conjugate dual layer scaffold decreased with increasing aqueous media exposure time when normalized to the fluorescence peak (Figure 4a) following an exponential decay (Figure 4b). The phosphorescence peak (525 nm) of the dye-polymer conjugate fibers was distinct compared to the dye (BF$_2$dbm(I)OH) polymer blend 85:15 PLAGA nanofibers (Figure 1c) after aqueous media exposure and did not see the same decrease during the first 7 days as the 50:50 PLAGA blend fibers (Figure 1a). This trend is expected based on known dye loading effects; gradual dye degradation in aqueous environments corresponds to lower dye to polymer loading and a decreased *P/F* ratio.[46] Scanning electron microscopy imaging showed that the slowly degrading support layer of the dual layer scaffold maintained consistent morphology over the 3 weeks and that the dye-polymer conjugate fibers swelled with time in aqueous media (Figure 4c—j). Unlike the blended dye polymer fibers, the phosphorescence peak of the dye-polymer conjugate fibers was more distinct from the low wavelength fluorescence signal (450 nm). Partial dye and polymer degradation did occur during the 21 day aqueous incubation; however, the peaks were still detectable in the dye-conjugate system (Figure 4a). To correct for reductions in phosphorescence intensity due to degradation of the fibers

in aqueous environments, a time-dependent scaling factor was applied to all data collected after day 0. The scaling factors were empirically defined from the degradation of the spectral signal after incubation of the dye-polymer conjugate nanofiber dual layer scaffold in aqueous media for given durations of time (Figure 4a,b).

Controlled low oxygen conditions help sensitive cells, such as stem cells, maintain their native phenotype longer in culture[47,48] or enhance differentiation *in vitro*.[49,50] To utilize the boron dye dual layer scaffold to detect hypoxia, the dependence of the *P/F* ratio on the oxygen tension was explored. The ability to measure oxygen, rather than simply sense a low oxygen condition, is desired since different cell types initiate hypoxic signaling at differing levels of oxygen.[51,52] Standard curves that relate the measured *P/F* ratio to known oxygen concentrations were constructed in dry and aqueous environments for the dye-polymer conjugate dual layer scaffold. The shape of the standard curves was similar regardless of whether data collection was performed directly at the sensor layer, through the support layer or in PBS (Figure 5a,b). Ratiometric readings were shifted in standard cell culture media (Dulbecco's Modified Eagle Medium, DMEM) compared to PBS (Figure 5c) likely due to the presence of phenol red, which has broad spectrum absorption, or may also be attributed in part to
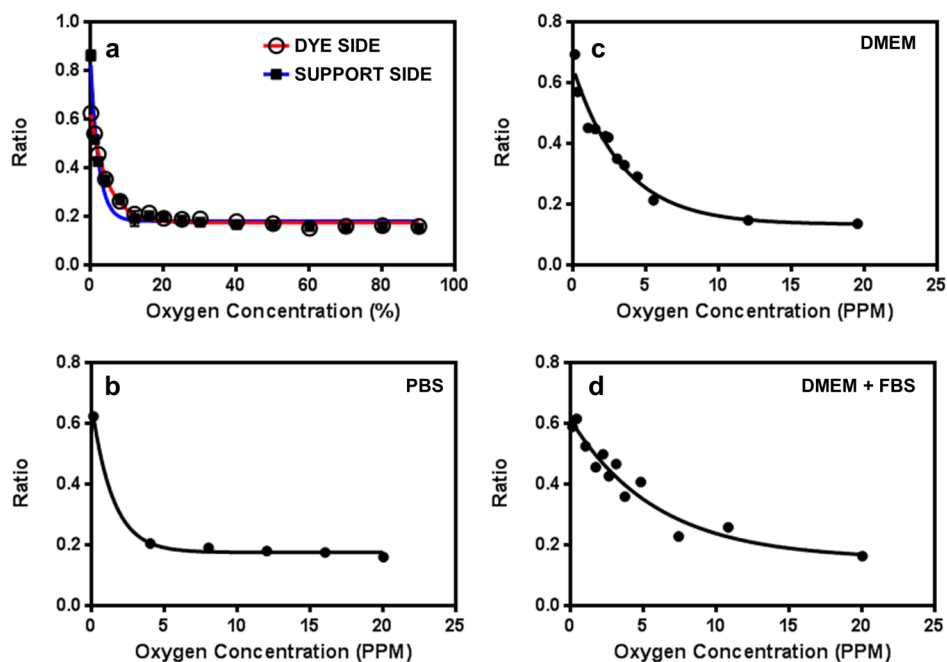
Figure 5. Calibration of the boron dye-polymer conjugate fibers is not affected by imaging through the support layer (a). Standard curves in the presence of aqueous media including PBS (b), DMEM (c), or DMEM + FBS (d) demonstrate function in physiological media. Oxygen concentration measured by percent for dry gas and parts per million (ppm) for aqueous conditions.

solvatochromism from the additional inorganic components that are not in PBS. The addition of fetal bovine serum (FBS) (Figure 5d) to DMEM demonstrates that biological entities (proteins, growth factors, *etc.*) do not change the curve shape, suggesting that the enhanced sensitivity below 10 ppm may be similar across tissue types and is attributable to the scaffold sensor material properties. Therefore, the hypoxia sensing scaffold signal would behave the same regardless of the tissue, since the physiological conditions (salinity, pH) are similar across tissue types while differing protein content does not affect the signal.

Spatiotemporal Oxygen Variations in Cell Culture. To ensure that the dye-polymer conjugated nanofiber sensor response is rapid enough in living systems, a moving stream of low oxygen gas was passed over dry fibers. The fibers in the nitrogen stream both activated (increased *P/F* ratio) and returned to baseline very quickly suggesting that the fibers could measure dynamic changes in local oxygen (Supporting Information Video 1). Biocompatibility of the nanofiber constructs was tested by culturing adherent NIH3T3 cells on the dye nanofiber layer. Tests showed no evidence of cytotoxicity as the majority of cells stained viable by fluorescein diacetate (FDA) (Figure 6a,c) and were not stained by propidium iodide (PI) (Figure 6b,c).

In vitro validation was conducted by seeding membrane stained D1 cells (adherent mouse bone marrow stem cell line) onto the scaffold. High-density layers of cells in culture are expected to consume oxygen in their local environment and therefore should create a scaffold level oxygen gradient. A corresponding spatial
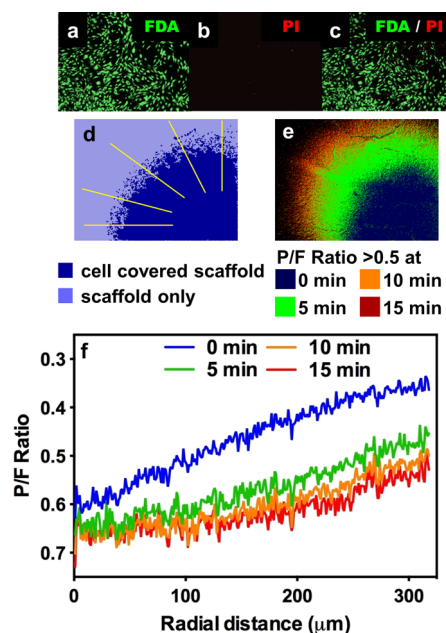
Figure 6. NIH3T3 cells were viable on the boron dye-polymer conjugate fibers ((a) viable fluorescein diacetate (FDA); (b) nonviable propidium iodide (PI); (c) overlay). The mean *P/F* ratio of 5 radial traces (d) from the center of the cell mass (1 μm resolution) indicate the ability of the dye-polymer conjugate nanofibers to detect a gradient from the cell-containing to the cell-devoid regions and the change in signal with time after the chamber is closed to environmental oxygen (e and f). ((e) colors indicate the scaffold area where the measured *P/F* ratio was greater than 0.5; (f) average of the 5 traces at indicated time point.)

change in the *P/F* reading of the boron dye-polymer conjugate nanofiber scaffold with increased time in a

Figure 7. Oxygenation varied with time (b and c) following implant of the dorsal skinfold window chamber ((a) standard error of the mean shown, $n = 8$, asterisk (*) indicates $p < 0.05$ by Student's t test *versus* days 0 through 2). Dye-polymer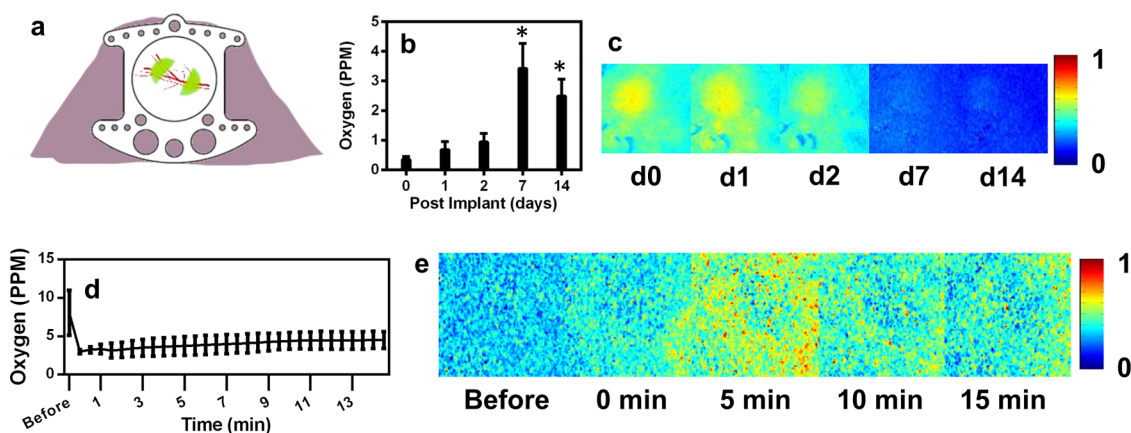 conjugate nanofibers show temporal variation in oxygen tension in transient *in vivo* ischemia ((d and e) experiment conducted at 2 weeks window chamber implant duration with a large thin dye-polymer conjugate layer only scaffold, $n = 3$).
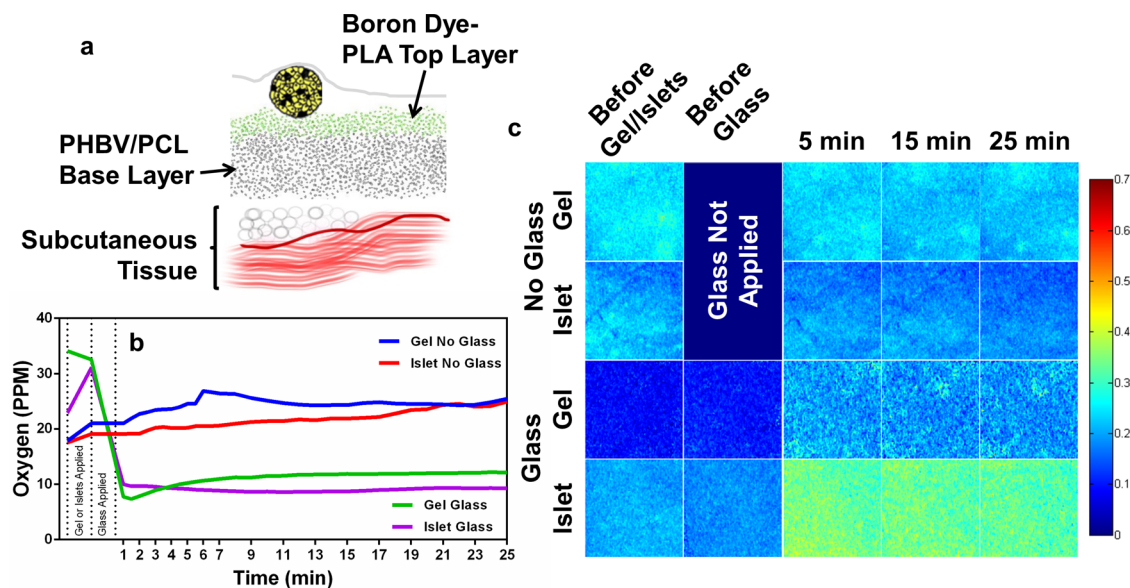

Figure 8. Pancreatic islets were placed on top of dye-polymer conjugate nanofibers in a gel in the dorsal skinfold window chamber ((a) cross-sectional schematic). A slightly reduced oxygen tension at steady state when islets were present in the gel was observed compared to the cell devoid gels ((b) $n = 3$ for each group, conducted on different days with correction to account for differing dye performance, $p > 0.05$). Representative ratiometric images (higher ratio indicates lower oxygen) of mice from each group are shown (c). Hypoxia developed quickly following replacement of glass coverslip.

closed environment would be expected. A cellular membrane stain was used to visualize the area of the nanofiber mat covered by cells (Figure 6d). The dual layer nanofiber scaffold with cells attached was mounted on a glass slide and sealed from the environment with a coverslip immediately prior to imaging to provide a barrier to diffusion of oxygen from the atmosphere. In the absence of this diffusion barrier, the P/F ratio did not change over time (data not shown). At time 0, lower *P/F* ratio (greater scaffold oxygen level) was detected farthest away from the central cell mass (Figure 6f, blue line), and the *P/F* ratio increased (oxygen level decreased) over time in the areas adjacent to the cells. As time increased from 0 to 15 min, the area experiencing higher *P/F* ratio (lower

oxygen) grew outward from the center of the adherent cells (Figure 6d—f). Nonuniform cell distribution upon the scaffold produces substantial variation in measurements, and therefore, measurements were binned by radial distance intervals of 50 μm to make comparisons between time and distance from the center of the cell-covered region (Supporting Information Figure S4a). Oxygen depletion is significant at 5 and 15 min from 50 to 300 μm. These data provide a biological proof of concept with spatial and temporal scaffold level variations observed.

Reoxygenation of Tissue after Injury. The dorsal skinfold window chamber (Figure 7a) was selected for *in vivo* validation as it provides a planar tissue surface that lends itself to intravital microscopy. The dye-polymer

conjugate dual layer scaffold was implanted and monitored in the window chamber for 14 days. The measured oxygen tension increased up to day 7 as the tissue recovered from the surgical procedure (Figure 7b,c) and oxygen gradients could be sensed in proximity to blood vessels (Supporting Information Figure S4b,c). Tissue oxygenation following ischemia initiated at $t = 0$ min initially decreased and then remained reduced (Figure 7d,e), showing the scaffold is tuned to a relevant range of dissolved oxygen *in vivo*.

Oxygenation of Islet Implants. Pancreatic islets are known to suffer from hypoxia due to their avascular multicellular spheroid shape.[53−56] To test the ability of the boron dye-conjugate nanofibers to detect acute changes in oxygenation of implanted islets, syngeneic pancreatic islets were isolated and directly transferred in a type 1 collagen gel onto the dual layer scaffold in the window chamber (Figure 8a). The *P/F* ratio demonstrates that the lowest oxygen level developed between 7 and 10 min following the delivery of the islets (Figure 8b,c). As in the *in vitro* cell experiments, the use of glass to seal the tissue compartment from contact with the open air was critical to see the effect of islet oxygen consumption to the end of the experiment. In both cases the islet containing gel was slightly more hypoxic than the acellular collagen gel. On the basis of these results, it is concluded that the dye−polymer conjugated fibers are well suited to a range of oxygen concentrations that arise in cell culture and *in vivo* models where hypoxia occurs.

CONCLUSION

Tissue engineering techniques have the potential to stimulate regeneration of damaged or diseased tissues; however, a major challenge is preventing cell death within thick constructs due to low oxygen tension. Although it is possible to study oxygen gradients in constructs or tissues using insertion of probes,[57] this disturbs the organization of growing cells and impedes the goal of monitoring scaffold cell interactions.[58] Scaffold based oxygen sensing is investigated here with boron dyes that emit a phosphorescence and fluorescence signal whose ratio changes with oxygen concentration, to overcome this drawback for construct study. Importantly, the nanofiber morphology of the dye-polymer conjugate scaffolds, obtained with careful parameter adjustments for the low molecular weight polymer, is an excellent substrate for cell attachment and growth. Cells attached to the dual layer scaffold *in vitro* cause spatial increases in the sensor output, suggesting oxygen tension variation on the millimeter scale as time increases. The first 2 to 3 weeks after a tissue engineering scaffold is implanted are crucial for successful implant integration, including vascularization. We showed increases in oxygenation as the tissue healed following dorsal skinfold chamber placement, with measurements out to 14 days. In conclusion, we have shown that this oxygen sensing scaffold is a platform for scientific investigation of changes in oxygenation within regenerative tissue engineering scaffolds.

METHODS

Electrospinning of Dye-Blend Nanofibers. The luminescent difluoroboron iodo-dibenzoylmethane dye (BF$_2$dbm(I)OH) was synthesized by the Fraser laboratory following previously published protocols.[10] Nanofiber meshes containing BF$_2$dbm(I)(OH) (referred to as dye and only used in the blend fibers) were fabricated by blending with polylactide-coglycolide (PLAGA, Lakeshore Biomaterials in two co-polymer ratios: 50/50 PLAGA (M_w = 65 kDa, PDI = 1.6) and 85/15 PLAGA (M_w = 109 kDa, PDI = 1.5)) and electrospinning. PLAGA (20% (w/v)), with the addition of 5% (w/w) of the dye, was dissolved in equal parts of tetrahydrofuran (THF) and dimethylformamide (DMF) (Fisher Scientific). This solution was loaded into a syringe, mounted into a programmable syringe pump (Aladdin-1000, World Precision Instruments, Sarasota, FL), and dispensed at a flow rate of 1 mL/h. A driving voltage of 15 kV was supplied to an 18G needle by a high voltage power source (Gamma High Voltage Research, Ormond Beach, FL) across a 15 cm collecting distance to a grounded aluminum collector plate. For imaging purposes, some fibers were collected on plasma-treated glass coverslips. Control PLAGA fibers were fabricated by the same methods, with an additional 5% (w/w) PLAGA to take the place of the dye in solution.

Electrospinning PHBV/PCL Fibers. Poly(hydroxylbutyrate-*co*-valerate) (PHBV, PHB 95/PHV 5; Carbomer, part no. 80181-31-3, lot no.11-SD658) and poly(caprolactone) (PCL; Sigma) were dissolved in equivalent amounts in 1:3 methanol/chloroform (Fisher Scientific) to yield an 18% weight-to-volume solution. The solution was loaded into a syringe mounted in a syringe pump (1 mL/h) suspended above an aluminum foil collecting plate in a sealed case. The metal blunt ended syringe tip was charged to 19 kV relative to ground and placed 14 cm above the collecting plate. The fibers were dried in a lyophilizer (Labconco, Kansas City, MO).

Electrospinning Dye-Polymer Conjugate (BF$_2$dbm(I)PLA). BF$_2$dbm(I)PLA (synthesized according to a previously published technique,[10] 13 kDa PLA) was dissolved in a solution of 10% pyridinium formate (PF; equimolar amounts of formic acid and pyridine), 20% ethanol, and 70% methylene chloride (Fisher Scientific, Waltham, MA) to yield a 30% weight-to-volume solution. The aluminum foil with dried PHBV/PCL fibers was used as the collecting plate for fabricating the dual-layer fibers, while a clean aluminum foil sheet was used to collect only BF$_2$dbm(I)PLA fibers. The BF$_2$dbm(I)PLA polymer solution was loaded into a syringe as described above and displaced at 1 mL/h. The metal syringe tip was charged to 25 kV relative to ground and placed 14.5 cm above the collecting plate. The fibers were dried in a lyophilizer.

Diameter Characterization. To image fibers, samples were mounted on 0.5 cm-diameter aluminum mounts. Mounted samples were gold-coated with a BAL-TEC SCD 005 Sputter Coater (BAL-TEC AG, Liechtenstein) for 210 s and observed under a scanning electron microscope (JEOL JSM-6400 SEM; Advanced Microscopy Facility, University of Virginia) at an accelerating voltage of 15 kV and magnification of 2000×. SEM images were acquired using ORION software to assess nanofiber morphology.

The diameters of the fibers were measured using ImageJ software (http://rsbweb.nih.gov/ij/). SEM images from each group were opened in ImageJ and a line was drawn across

the center of the image. 50 diameter measurements were taken from nanofibers intercepting the line.

Hydrophobicity Characterization. Hydrophobicity of each nanofiber condition was quantified through contact angle measurements. A drop of deionized water was placed on top of the nanofibers for each condition. A goniometer (Rame-Hart Standard Contact Angle Goniometer, Model 200; Rame-Hart Instrument Co., Succasunna, NJ) and DROPimage Standard software were used to measure the contact angle between the fiber and the liquid. Contact angle measurements were repeated three times for each type of nanofiber.

Strength Characterization. To characterize nanofiber strength, three samples from each nanofiber condition (except BF_2dbm(I)PLA) were subjected to tensile strength testing using an Instron materials testing instrument (Instron Model 5543; Instron Worldwide Headquarters, Norwood, MA). The BlueHill2 Program Software (version 2.14) was used to obtain force—displacement graphs for each sample. Dimensions of each sample (length, width, thickness) were measured prior to testing. The force—displacement curve data was used to calculate engineering stress and strain; stress (MPa) was calculated by dividing load (N) by cross-sectional area (width × thickness; mm^2) of the sample at each time point. Strain was calculated by evaluating the percent extension, or extension (mm) divided by length (mm), at each time point. Stress—strain curves were plotted for each sample. Ultimate Tensile Strength (UTS) was determined by the highest point on the stress—strain curve. Young's Modulus (E) was determined by regression fitting the linear region on the stress—strain curve and evaluating the slope. Values for E and UTS were averaged across samples for each condition. An independent means t test was conducted to assess the strength differences between the two conditions. BF_2dbm(I)PLA fibers were not subjected to strength testing due to the inability to remove fibers from collecting foil.

Ratiometric Imaging. To test the oxygen-sensing capabilities of the dual-layer fibers (BF_2dbm(I)PLA fibers on PHBV/PCL fibers), a section of the fibers was cut from collecting foil. The dual-layer fibers were then peeled from the foil after soaking in EtOH and air-dried. Then, the dual-layer section was taped to the bottom of a plastic, nontissue-culture Petri dish. To image the BF_2dbm(I)PLA fiber layer, the dual-layer fibers were exposed to UV light (395−415 nm) from a fluorescence lamp (X-Cite 120Q; Lumen Dynamics Group, Inc., Ontario, Canada). Then, the fluorescence and phosphorescence modes of emission were collected with a Beta-Lactamase Filter 1 (440−480 nm) and Beta-Lactamase Filter 2 (485−515 nm) (Chroma Technology Corp; Bellows Falls, VT), respectively, for the same area at a constant exposure time (4.5 or 25 ms for boron dye side facing objective or support layer facing objective respectively) and lamp intensity level (lowest setting). Images were taken at 10× magnification on an inverted microscope (Microscope Axio Observer.A1; Carl Zeiss, Bulgaria) with an AxioCam HSM camera (Carl Zeiss). Once an area was imaged while air-exposed, nitrogen was blown into the Petri dish through a pipet tip for 5 min before imaging the same area. Then, a new area was chosen and the Petri dish was exposed to only air for 5 min before being imaged. This was repeated for five different areas.

To generate the ratiometric images, the separate fluorescence and phosphorescence intensity images for a single area were loaded into MATLAB. The phosphorescence-to-fluorescence intensity ratio was calculated at each pixel (pixels with zero fluorescence intensity were skipped in all calculations). To quantify the phosphorescence-to-fluorescence ratio for an entire condition (air-exposed vs nitrogen-exposed), all five sets of fluorescence and phosphorescence images were loaded into MATLAB. The average intensity was calculated for each image, and then the phosphorescence-to-fluorescence ratio was calculated by dividing average phosphorescence by average fluorescence intensities for each field of view imaged. Finally, the five phosphorescence-to-fluorescence ratios were averaged and compared between conditions.

Standard Curves. A section of the dual-layer fibers were cut, removed from the foil, and taped to the bottom of a Petri dish. Two holes were cut into opposite sides of the dish and one hole was cut into the cover. The Petri dish was placed onto the stage of an inverted microscope and gas inlet and outlet hoses were

attached to the holes on the side of the dish. The probe of an oxygen sensor (Oxygen Analyzer Model 600; Engineered Systems & Designs, Inc., Newark, DE) was placed over the hole in the top of the Petri dish. The gas inlet hose was connected to a mixing chamber, which was connected to an oxygen tank and a nitrogen tank. The gas outlet was connected to a flask open to the atmosphere. The entire setup is depicted in Supporting Information Figure S5. The outputs of the oxygen and nitrogen tanks were adjusted such that the reading on the oxygen sensor was stable at the following oxygen concentrations: 1.0, 2.0, 4.0, 8.0, 12.0, 16.0, 20.0, 25.0, 30.0, 40.0, 50.0, 60.0, 70.0, 80.0, and 90.0%. When the oxygen concentration was stable, fluorescence and phosphorescence images were taken for five different spots. The imaging procedure was the same for the various conditions except that the exposure time for direct imaging of the BF_2dbm(I)PLA side was 31.8 ms and for indirect imaging was 68.8 ms. The images were then loaded into MATLAB. For each oxygen concentration and spot imaged, the average phosphorescence intensity was divided by the average fluorescence intensity to obtain the phosphorescence-to-fluorescence ratio. Then, the five ratios were averaged for each oxygen concentration.

Oxygen Tension of Adherent Cells. D1 cells (obtained from a colleague at UVA, also deposited at ATCC, CRL-12424) were cultured in DMEM (Invitrogen, Grand Island, NY) supplemented with fetal bovine serum, penicillin, and streptomycin. Sections (1 cm × 1 cm) of dual-layer dye-polymer conjugate fibers were cut and removed from the collecting foil and placed in multiwell nontissue culture plates (BD, Franklin Lakes, NJ). Cells were stained with DiD and were placed on the center of the fiber section in a 10-μL droplet (5×10^6 cells). The well-plates were placed in the incubator for 1 h to allow the cells to adhere to the fibers, followed by flooding with media and being placed back in the incubator. Next fiber sections were placed on glass slides and covered and sealed with a glass coverslip, which not only accelerated the time required for the cells to consume a measurable amount of the oxygen available to them, but also flattened the nanofibers so that reasonably focused images could be obtained. One spot was chosen for each section and imaged at 0, 5, 10, and 15 min after sealing. DiD, oxygen sensor fluorescence, and oxygen sensor phosphorescence images were captured at 4× magnification with a Cy5 filter, Beta-Lactamase Filter 1, and Beta-Lactamase Filter 2, respectively.

The phosphorescence-to-fluorescence ratio was calculated for each pixel. Ratio measurements along radial traces were captured using ImageJ. Five lines were drawn which radiated from the lower right corner of the images at 0, 5, 10, and 15 min. Data was then averaged from these 5 traces and displayed in 50 μm length bins with standard deviation to indicate the spatial variability. A two way ANOVA was used to test for significance.

Degradation Study. Sections (1 cm × 1 cm) of dual-layer dye-polymer conjugate fibers were cut and removed from the collecting foil and placed in PBS in polycarbonate vials. The vials were incubated at 37 °C in a water bath with circular agitation for 0, 7, 14, or 21 days. After removal of the fibers from the water bath and PBS, the fibers were dried in a lyophilizer. Then, six samples from each time point were placed and sealed in glass scintillation vials with Teflon lids under nitrogen in a glovebox. The emission spectrum (400−700 nm) of each sample was obtained using a UV−vis spectrophotometer (Hewlett-Packard 8452A diode-array). All emission spectra were normalized to the fluorescence peak and the six spectra from each time point were averaged together.

Gel Permeation Chromatography. Samples were dissolved in HPLC-grade tetrahydrofuran (THF), filtered through a 0.2 μm filter, and loaded into vials with a septum for gel permeation chromatography analysis (GPC). Molecular weight was measured by GPC (THF, 20 °C, 1.0 mL/min) against polystyrene standards on a Hewlett-Packard instrument (series 1100 HPLC) equipped with Polymer Laboratories 5 μm mixed-C columns and connected to a refractive index (Viscotek LR 40) detector. Data were processed with the OmniSEC software (version 4.2, Viscotek Corp).

Pancreatic Islet Isolation. Pancreatic islets were isolated from C57BL/6 mice (Jackson Laboratories, Bar Harbor, ME) that were sacrificed immediately prior to the procedure. After confirmation of euthanasia, a lateral incision exposed the peritoneal cavity and two lobes of the liver were placed onto sterile gauze over the animal's ribcage. The common bile duct was occluded by tying off with suture at the entrance to the intestine and was cannulated with a 30G needle for injection of 2−3 mL of 1.4 mg/mL collagenase P (Roche) dissolved in Hank's Balanced Salt Solution (HBSS, Thermo Scientific) supplemented with 10 g/L heat treated bovine serum albumin and 0.35g/L sodium bicarbonate (supplemented HBSS). The pancreas was carefully removed from the animal after distension and placed in 1 mL of supplemented HBSS on ice to which 4 mL of enzyme solution was added in individual 15 mL centrifuge tubes for each mouse. Incubation in a 37 °C water bath (15 min was selected with this batch of enzyme) was followed by vigorous shaking by hand to disrupt tissue structure. Next the tubes were placed immediately on ice and the balance of the 15 mL was filled with supplemented HBSS. Two washes in supplemented HBSS were followed by a filtering through a steel mesh and density separation with Histopaque 1077 (Sigma #10771). Two more washes and a wash in fully supplemented culture media (RPMI1640 + 10% FBS, 2% penicillin streptomycin + 2.5% 1× HEPES) completed the isolation. The islets were placed onto ice in 50 mL tubes containing 10 mL of media and transported to another building for the *in vivo* experiment 4 h after isolation completion.

Dorsal Skinfold Window Chamber Experiments. All surgeries were performed according to a protocol approved by the Institutional Animal Care Committee at the University of Virginia. Eighteen C57BL/6 mice (Jackson Laboratories, Bar Harbor, ME) were used. Anesthesia was induced with isoflurane gas (2−3%) and the surgical plane was maintained throughout the procedure with a nose cone (1−2%) equipped with a scavenging apparatus. Briefly, dorsal skin was attached to a corkboard with 26 gauge needles and the top layer of skin corresponding with the window portion of the chamber (10 mm diameter) was removed to expose the cutaneous microcirculation of the panniculus carnosus. Ringers solution was added throughout the process to keep the area hydrated. The top titanium chamber was secured with sutures and the screws were tightened to hold the chamber together. Ringers solution was used to fill the cavity before implanting two 6 mm diameter dye-polymer conjugate dual layer nanofiber scaffold hemispheres and applying the glass coverslip. Postoperative bupronex was administered to the animals every 12 h for 48 h.

Microscopy color CCD images (Nikon, Melville, NY) were taken on Days 0, 1, 2, 7, and 14 after surgery using unfiltered brightfield light or UV excitation with a color CCD camera mounted on a stereomicroscope. Excitation was from a hand-held UV lamp.

For the 2 weeks following implants, the entire window chamber was imaged and the implant area was manually cropped and quantified to produce a mean value for each of eight mice, bars show standard error of the mean. Cold type 1 rat tail collagen (Becton-Dickinson), with or without islets, was placed on the exposed tissue and nanofibers at $t = 0$ min. At 2 weeks, a transient ischemia in 3 separate mice was created by placing clamps on the skin which is tented up outside the two pieces of the dorsal skinfold window chamber at $t = 0$ min. These mice had fibers collected on the coverslip that closes the window chamber rather than the dual layer fiber scaffold. Exposure time was 1 ms for the color images.

***In Vivo* Image Analysis.** Because no filters were used during the *in vivo* experiments, the two sensor emissions were distinguished solely on the basis of the green (phosphorescence) and blue (fluorescence) channels of color images. The basic image reading and ratio calculations that were used for the *in vitro* experiments were used for the *in vivo* experiments, with the exception being that it was channels of a single color image rather than two separate grayscale images as the inputs. For quantification, areas of the images that did not include sensor nanofibers were excluded from the analysis. Pixels that had an undefined ratio (due to a lack of fluorescence) were also excluded from the analysis. To correct for reductions in phosphorescence intensity due to degradation of the fibers in aqueous environments, a time-dependent scaling factor was applied to all data collected after day 0. Scaling factor was determined based on the change in the max intensity phosphorescence signal over time from the *in vitro* degradation and spectral analysis (Figure 4b). Curve fitting to the degradation data provides scaling factors specific to each time point.

In addition, a correction factor was applied to all images where the glass was present during imaging (1.56 for all time points with glass coverslip applied). The glass correction factor was determined by imaging unused fibers, laying a glass coverslip over the fibers and immediately imaging a second time. When the glass covered image average was multiplied by the glass correction factor of 1.56 (SD 0.06, $n = 4$), the measured ratio was increased back to that found without the glass covering the area. In this way, all *in vivo* ratio values were scaled to be comparable to Day 0 values without the glass coverslip over the window chamber.

Statistics. The Student's *t* test or two way ANOVA are used for determining significance at a $p < 0.05$.

Conflict of Interest: The authors declare no competing financial interest.

Supporting Information Available: Scanning electron micrographs, *in vivo* images, *in vitro* experimental setup diagram, oxygenation data, tabulated material characteristics, and a nitrogen stream video (avi) file. This material is available free of charge *via* the Internet at http://pubs.acs.org.

REFERENCES AND NOTES

1. Semenza, G. L. Oxygen Sensing, Homeostasis, and Disease. *N. Engl. J. Med.* **2011**, *365*, 537–547.
2. Franke, K.; Gassmann, M.; Wielockx, B. Erythrocytosis: The HIF Pathway in Control. *Blood* **2013**, *122*, 1122–1128.
3. Pietrocola, F.; Izzo, V.; Niso-Santano, M.; Vacchelli, E.; Galluzzi, L.; Maiuri, M. C.; Kroemer, G. Regulation of Autophagy by Stress-Responsive Transcription Factors. *Semin. Cancer Biol.* **2013**, *23*, 310–322.
4. Ratcliffe, P. J. Oxygen Sensing and Hypoxia Signalling Pathways in Animals: The Implications of Physiology for Cancer. *J. Physiol. (Oxford, U. K.)* **2013**, *591*, 2027–2042.
5. Escribese, M. M.; Casas, M.; Corbí, A. L. Influence of Low Oxygen Tensions on Macrophage Polarization. *Immunobiology* **2012**, *217*, 1233–1240.
6. Phelps, E. A.; García, A. J. Engineering More Than a Cell: Vascularization Strategies in Tissue Engineering. *Curr. Opin. Biotechnol.* **2010**, *21*, 704–709.
7. Kannan, R. Y.; Salacinski, H. J.; Sales, K.; Butler, P.; Seifalian, A. M. The Roles of Tissue Engineering and Vascularisation in the Development of Micro-Vascular Networks: A Review. *Biomaterials* **2005**, *26*, 1857–1875.
8. Xu, H.; Aylott, J. W.; Kopelman, R.; Miller, T. J.; Philbert, M. A. A Real-Time Ratiometric Method for the Determination of Molecular Oxygen Inside Living Cells Using Sol-Gel-Based Spherical Optical Nanosensors with Applications to Rat C6 Glioma. *Anal. Chem.* **2001**, *73*, 4124–4133.
9. Koo, Y.-E. L.; Cao, Y.; Kopelman, R.; Koo, S. M.; Brasuel, M.; Philbert, M. A. Real-Time Measurements of Dissolved Oxygen Inside Live Cells by Organically Modified Silicate Fluorescent Nanosensors. *Anal. Chem.* **2004**, *76*, 2498–2505.

10. Zhang, G.; Palmer, G. M.; Dewhirst, M. W.; Fraser, C. L. A Dual-Emissive-Materials Design Concept Enables Tumour Hypoxia Imaging. *Nat. Mater.* **2009**, *8*, 747–751.

11. Pfister, A.; Zhang, G.; Zareno, J.; Horwitz, A. F.; Fraser, C. L. Boron Polylactide Nanoparticles Exhibiting Fluorescence and Phosphorescence in Aqueous Medium. *ACS Nano* **2008**, *2*, 1252–1258.

12. Kersey, F. R.; Zhang, G.; Palmer, G. M.; Dewhirst, M. W.; Fraser, C. L. Stereocomplexed Poly(lactic acid)-Poly-(ethylene glycol) Nanoparticles with Dual-Emissive Boron Dyes for Tumor Accumulation. *ACS Nano* **2010**, *4*, 4989–4996.

13. Mosinger, J.; Lang, K.; Plístil, L.; Jesenská, S.; Hostomský, J.; Zelinger, Z.; Kubát, P. Fluorescent Polyurethane Nanofabrics: A Source of Singlet Oxygen and Oxygen Sensing. *Langmuir* **2010**, *26*, 10050–10056.

14. Songzhu, L.; Xiangting, D.; Jinxian, W.; Guixia, L.; Wenshen, Y.; Ruokun, J. Fabrication of Eu(III) Complex Doped Nanofibrous Membranes and Their Oxygen-Sensing Properties. *Spectrochim. Acta, Part A* **2010**, *77*, 885–889.

15. Wen, C.; Tao, G.; Xu, X.; Feng, X.; Luo, R. A Phosphorescent Copper(I) Complex: Synthesis, Characterization, Photophysical Property, and Oxygen-Sensing Behavior. *Spectrochim. Acta, Part A* **2011**, *79*, 1345–1351.

16. Zhang, H.; Lei, B.; Dong, H.; Liu, Y. Oxygen Sensing Properties of Cu(I) Complex/Polystyrene Composite Nanofibers Prepared by Electrospinning. *J. Nanosci. Nanotechnol.* **2011**, *11*, 9840–9845.

17. Hong, H.; Zhu, L.; Wang, A.; Lu, H. Re(I) Complex Doped Nanofibers for Oxygen Optical Sensing. *Spectrochim. Acta, Part A* **2012**, *98*, 466–473.

18. Xue, R.; Behera, P.; Viapiano, M. S.; Lannutti, J. J. Rapid Response Oxygen-Sensing Nanofibers. *Mater. Sci. Eng., C* **2013**, *33*, 3450–3457.

19. Dahlin, R. L.; Kasper, F. K.; Mikos, A. G. Polymeric Nanofibers in Tissue Engineering. *Tissue Eng., Part B* **2011**, *17*, 349–364.

20. Ren, Y.-J.; Zhang, S.; Mi, R.; Liu, Q.; Zeng, X.; Rao, M.; Hoke, A.; Mao, H.-Q. Enhanced Differentiation of Human Neural Crest Stem Cells Towards the Schwann Cell Lineage by Aligned Electrospun Fiber Matrix. *Acta Biomater.* **2013**, *9*, 7727–7736.

21. Mukhatyar, V. J.; Salmerón-Sánchez, M.; Rudra, S.; Mukhopadaya, S.; Barker, T. H.; García, A. J.; Bellamkonda, R. V Role of Fibronectin in Topographical Guidance of Neurite Extension on Electrospun Fibers. *Biomaterials* **2011**, *32*, 3958–3968.

22. Lee, S.; Leach, M. K.; Redmond, S. A.; Chong, S. Y. C.; Mellon, S. H.; Tuck, S. J.; Feng, Z.-Q.; Corey, J. M.; Chan, J. R. A Culture System to Study Oligodendrocyte Myelination Processes Using Engineered Nanofibers. *Nat. Methods* **2012**, *9*, 917–922.

23. Silva, G. A.; Czeisler, C.; Niece, K. L.; Beniash, E.; Harrington, D. A.; Kessler, J. A.; Stupp, S. I. Selective Differentiation of Neural Progenitor Cells by High-Epitope Density Nanofibers. *Science (Washington, DC, U.S.)* **2004**, *303*, 1352–1355.

24. Xie, J.; Willerth, S. M.; Li, X.; Macewan, M. R.; Rader, A.; Sakiyama-Elbert, S. E.; Xia, Y. The Differentiation of Embryonic Stem Cells Seeded on Electrospun Nanofibers into Neural Lineages. *Biomaterials* **2009**, *30*, 354–362.

25. Neal, R. A.; Tholpady, S. S.; Foley, P. L.; Swami, N.; Ogle, R. C.; Botchwey, E. A. Alignment and Composition of Laminin-Polycaprolactone Nanofiber Blends Enhance Peripheral Nerve Regeneration. *J. Biomed. Mater. Res., Part A* **2011**, *100A*, 406–423.

26. Hsiao, C.-W.; Bai, M.-Y.; Chang, Y.; Chung, M.-F.; Lee, T.-Y.; Wu, C.-T.; Maiti, B.; Liao, Z.-X.; Li, R.-K.; Sung, H.-W. Electrical Coupling of Isolated Cardiomyocyte Clusters Grown on Aligned Conductive Nanofibrous Meshes for Their Synchronized Beating. *Biomaterials* **2013**, *34*, 1063–1072.

27. Yeo, M.; Lee, H.; Kim, G. Three-Dimensional Hierarchical Composite Scaffolds Consisting of Polycaprolactone, β-Tricalcium Phosphate, and Collagen Nanofibers: Fabrication, Physical Properties, and *in Vitro* Cell Activity for Bone Tissue Regeneration. *Biomacromolecules* **2011**, *12*, 502–510.

28. Kumbar, S. G.; Nukavarapu, S. P.; James, R.; Nair, L. S.; Laurencin, C. T. Electrospun Poly(lactic acid-co-glycolic acid) Scaffolds for Skin Tissue Engineering. *Biomaterials* **2008**, *29*, 4100–4107.

29. McClendon, M. T.; Stupp, S. I. Tubular Hydrogels of Circumferentially Aligned Nanofibers To Encapsulate and Orient Vascular Cells. *Biomaterials* **2012**, *33*, 5713–5722.

30. Yamazoe, T.; Shiraki, N.; Toyoda, M.; Kiyokawa, N.; Okita, H.; Miyagawa, Y.; Akutsu, H.; Umezawa, A.; Sasaki, Y.; Kume, K.; et al. A Synthetic Nanofibrillar Matrix Promotes in Vitro Hepatic Differentiation of Embryonic Stem Cells and Induced Pluripotent Stem Cells. *J. Cell Sci.* **2013**, *126*, 5391–5399.

31. Thibault, R. A.; Scott Baggett, L.; Mikos, A. G.; Kasper, F. K. Osteogenic Differentiation of Mesenchymal Stem Cells on Pregenerated Extracellular Matrix Scaffolds in the Absence of Osteogenic Cell Culture Supplements. *Tissue Eng., Part A* **2010**, *16*, 431–440.

32. Gershovich, J. G.; Dahlin, R. L.; Kasper, F. K.; Mikos, A. G. Enhanced Osteogenesis in Cocultures with Human Mesenchymal Stem Cells and Endothelial Cells on Polymeric Microfiber Scaffolds. *Tissue Eng. Part A* **2013**, *19*, 2565–2576.

33. Cohen-Karni, T.; Jeong, K. J.; Tsui, J. H.; Reznor, G.; Mustata, M.; Wanunu, M.; Graham, A.; Marks, C.; Bell, D. C.; Langer, R.; et al. Nanocomposite Gold-Silk Nanofibers. *Nano Lett.* **2012**, *12*, 5403–5406.

34. Das, A.; Segar, C. E.; Hughley, B. B.; Bowers, D. T.; Botchwey, E. A. The Promotion of Mandibular Defect Healing by the Targeting of S1P Receptors and the Recruitment of Alternatively Activated Macrophages. *Biomaterials* **2013**, *34*, 9853–9862.

35. Nur-E-Kamal, A.; Ahmed, I.; Kamal, J.; Schindler, M.; Meiners, S. Three-Dimensional Nanofibrillar Surfaces Promote Self-Renewal in Mouse Embryonic Stem Cells. *Stem Cells* **2006**, *24*, 426–433.

36. Hashemi, S. M.; Soudi, S.; Shabani, I.; Naderi, M.; Soleimani, M. The Promotion of Stemness and Pluripotency Following Feeder-Free Culture of Embryonic Stem Cells on Collagen-Grafted 3-Dimensional Nanofibrous Scaffold. *Biomaterials* **2011**, *32*, 7363–7374.

37. Kingham, E.; Oreffo, R. O. C. Embryonic and Induced Pluripotent Stem Cells: Understanding, Creating, and Exploiting the Nano-Niche for Regenerative Medicine. *ACS Nano* **2013**, *7*, 1867–1881.

38. Ardeshirylajimi, A.; Hosseinkhani, S.; Parivar, K.; Yaghmaie, P.; Soleimani, M. Nanofiber-Based Polyethersulfone Scaffold and Efficient Differentiation of Human Induced Pluripotent Stem Cells into Osteoblastic Lineage. *Mol. Biol. Rep.* **2013**, *40*, 4287–4294.

39. Murray, R. A.; Zhang, G.; Harmata, D.; Neal, R. A.; Botchwey, E. A.; Fraser, C. L. Fabrication and Degradation of Nanofibers Based on Luminescent Boron Dye-PLGA Blends. In *Biomaterials*; American Chemical Society: Washington D. C., 2010; pp 33−42.

40. Liu, W.; Thomopoulos, S.; Xia, Y. Electrospun Nanofibers for Regenerative Medicine. *Adv. Healthcare Mater.* **2012**, *1*, 10–25.

41. Miller, R. A.; Brady, J. M.; Cutright, D. E. Degradation Rates of Oral Resorbable Implants (Polylactates and Polyglycolates): Rate Modification with Changes in PLA/PGA Copolymer Ratios. *J. Biomed. Mater. Res.* **1977**, *11*, 711–719.

42. Sun, H.; Scharff-Poulsen, A. M.; Gu, H.; Almdal, K. Synthesis and Characterization of Ratiometric, pH Sensing Nanoparticles with Covalently Attached Fluorescent Dyes. *Chem. Mater.* **2006**, *18*, 3381–3384.

43. Nam, J.; Johnson, J.; Lannutti, J. J.; Agarwal, S. Modulation of Embryonic Mesenchymal Progenitor Cell Differentiation *via* Control Over Pure Mechanical Modulus in Electrospun Nanofibers. *Acta Biomater.* **2011**, *7*, 1516–1524.

44. Kai, D.; Prabhakaran, M. P.; Stahl, B.; Eblenkamp, M.; Wintermantel, E.; Ramakrishna, S. Mechanical Properties and *in Vitro* Behavior of Nanofiber-Hydrogel Composites

for Tissue Engineering Applications. *Nanotechnology* **2012**, *23*, 095705.

45. Jiang, X.; Nai, M. H.; Lim, C. T.; Le Visage, C.; Chan, J. K. Y.; Chew, S. Y. Polysaccharide Nanofibers with Variable Compliance for Directing Cell Fate. *J. Biomed. Mater. Res., Part A* **2014**, 10.1002/jbm.a.35237.

46. Zhang, G.; Kooi, S. E.; Demas, J. N.; Fraser, C. L. Emission Color Tuning with Polymer Molecular Weight for Difluoroboron Dibenzoylmethane-Polylactide. *Adv. Mater. (Weinheim, Ger.)* **2008**, *20*, 2099–2104.

47. Forristal, C. E.; Christensen, D. R.; Chinnery, F. E.; Petruzzelli, R.; Parry, K. L.; Sanchez-Elsner, T.; Houghton, F. D. Environmental Oxygen Tension Regulates the Energy Metabolism and Self-Renewal of Human Embryonic Stem Cells. *PLoS One* **2013**, *8*, e62507.

48. Grayson, W. L.; Zhao, F.; Izadpanah, R.; Bunnell, B.; Ma, T. Effects of Hypoxia on Human Mesenchymal Stem Cell Expansion and Plasticity in 3D Constructs. *J. Cell. Physiol.* **2006**, *207*, 331–339.

49. Bath, C.; Yang, S.; Muttuvelu, D.; Fink, T.; Emmersen, J.; Vorum, H.; Hjortdal, J.; Zachar, V. Hypoxia Is a Key Regulator of Limbal Epithelial Stem Cell Growth and Differentiation. *Stem Cell Res.* **2013**, *10*, 349–360.

50. Stacpoole, S. R. L.; Webber, D. J.; Bilican, B.; Compston, A.; Chandran, S.; Franklin, R. J. M. Neural Precursor Cells Cultured at Physiologically Relevant Oxygen Tensions Have a Survival Advantage Following Transplantation. *Stem Cells Transl. Med.* **2013**, *2*, 464–472.

51. McKeown, S. R. Defining Normoxia, Physoxia and Hypoxia in Tumours-Implications for Treatment Response. *Br. J. Radiol.* **2014**, *87*, 20130676.

52. Carreau, A.; El Hafny-Rahbi, B.; Matejuk, A.; Grillon, C.; Kieda, C. Why Is the Partial Oxygen Pressure of Human Tissues a Crucial Parameter? Small Molecules and Hypoxia. *J. Cell. Mol. Med.* **2011**, *15*, 1239–1253.

53. Buchwald, P. FEM-Based Oxygen Consumption and Cell Viability Models for Avascular Pancreatic Islets. *Theor. Biol. Med. Model.* **2009**, *6*, 5.

54. Ludwig, B.; Rotem, A.; Schmid, J.; Weir, G. C.; Colton, C. K.; Brendel, M. D.; Neufeld, T.; Block, N. L.; Yavriyants, K.; Steffen, A.; *et al.* Improvement of Islet Function in a Bioartificial Pancreas by Enhanced Oxygen Supply and Growth Hormone Releasing Hormone Agonist. *Proc. Natl. Acad. Sci. U. S. A.* **2012**, *109*, 5022–5027.

55. Pedraza, E.; Coronel, M. M.; Fraker, C. A.; Ricordi, C.; Stabler, C. L. Preventing Hypoxia-Induced Cell Death in Beta Cells and Islets *via* Hydrolytically Activated, Oxygen-Generating Biomaterials. *Proc. Natl. Acad. Sci. U. S. A.* **2012**, *109*, 4245–4250.

56. Wilson, J. T.; Cui, W.; Chaikof, E. L. Layer-by-Layer Assembly of a Conformal Nanothin PEG Coating for Intraportal Islet Transplantation. *Nano Lett.* **2008**, *8*, 1940–1948.

57. Duling, B. R.; Berne, R. M. Longitudinal Gradients in Periarteriolar Oxygen Tension. A Possible Mechanism for the Participation of Oxygen in Local Regulation of Blood Flow. *Circ. Res.* **1970**, *27*, 669–678.

58. Allen, J.; Liu, Y.; Kim, Y. L.; Turzhitsky, V. M.; Backman, V.; Ameer, G. A. Spectroscopic Translation of Cell-Material Interactions. *Biomaterials* **2007**, *28*, 162–174.